A Functional Floxed Allele of *Pkd1* that Can Be Conditionally Inactivated *In Vivo*

KLAUS B. PIONTEK,* DAVID L. HUSO,† ALEXANDER GRINBERG,‡ LIJUAN LIU,* DJAHIDA BEDJA,† HAIDAN ZHAO,§ KATHLEEN GABRIELSON,† FENG QIAN,* CHANGLIN MEI,§ HEINER WESTPHAL,‡ and GREGORY G. GERMINO*

*Departments of *Medicine and †Comparative Medicine, Johns Hopkins University School of Medicine, Baltimore, Maryland; ‡Laboratory of Mammalian Genes and Development, National Institute of Child Health and Human Development, National Institutes of Health, Bethesda, Maryland; and §Department of Medicine, Shanghai Changzheng Hospital, Shanghai, China*

Abstract. Gene targeting has been used to create a variety of lines of mice with *Pkd1* mutations that share many common features. Homozygous *Pkd1* mutants invariably develop pancreatic and renal cysts if they survive to day 15.5 post coitum and die in either the fetal or the perinatal period. In contrast, mice with heterozygous mutations of *Pkd1* are generally normal and have few if any renal cysts. These features have limited the utility of these models as tools to study the pathogenesis of cyst formation and the effect of various therapeutic interventions on disease progression. This report describes a new line of mice with a floxed allele of *Pkd1* ($Pkd1^{cond}$) that has an FRT-flanked neomycin cassette inserted into intron 1 and lox P sites inserted into intron 1 and intron 4. The $Pkd1^{cond}$ allele is fully functional, and homozygotes are viable and healthy. It is shown that the lox P and FRT sites can be selectively induced to recombine to produce two new alleles, $Pkd1^{del2-4}$ and $Pkd1^{cond\text{-}\Delta neo}$, by crossing to animals that express either the cre or FLPe recombinase, respectively. It is found that $Pkd1^{del2-4}$ allele functions as a true null, whereas presence or absence of the neomycin gene has no functional effects. It also is shown that somatic loss of *Pkd1* results in renal and hepatic cysts. This new line of mice will be invaluable in the study of *Pkd1* biology and serve as a powerful new tool that can be used to study the pathogenesis of autosomal dominant polycystic kidney disease.

Autosomal dominant polycystic kidney disease (ADPKD) in humans is characterized by a slowly progressive course in which cysts increase in size and number throughout the lifetime of an individual (1,2). Molecular genetic studies of human cystic epithelial cells suggest that the disease is recessive on a molecular level (3). However, it is not presently known whether somatic mutations are acquired during the lifetime of an individual or during the relatively brief period of fetal development, at a time of relatively rapid growth and cellular proliferation. Distinguishing between these two possibilities has important implications for understanding the pathophysiology of the disease and for the development of future therapeutic approaches. The results also have important implications for our understanding of the role of polycystins in renal tubulogenesis.

A number of mouse lines with targeted mutations of either *Pkd1* or *Pkd2* have been described (4–8). Regardless of which gene is inactivated, the different mouse lines share many common features. Homozygous inactivation of either gene results in bilateral renal cyst formation beginning at approximately embryonic day 15.5 (E15.5; the presence of a vaginal plug being defined as E0.5d) and invariably results in fetal or perinatal demise. In contrast, mice with heterozygous mutations of *Pkd1* or *Pkd2* are generally normal and have few if any renal cysts, although hepatic cysts often are a late presentation. Although these studies have shown conclusively that *Pkd1* and *Pkd2* are required for the establishment of normal renal tubular morphology, the severity of the presentation associated with the homozygous null state coupled with the relatively benign status of heterozygosity has limited their utility.

Wu *et al.* (9) reported an exceptionally useful line of animals that had a local duplication of the 5' end of *Pkd2* that resulted from gene targeting. This fortuitous event resulted in an unstable allele that when combined with a *Pkd2* null allele resulted in animals with renal and hepatic disease of variable severity that closely mimics human ADPKD. Despite its unique properties, this model has several features that limit its usefulness to explore the pathobiology of *Pkd2*: Somatic mutation is random and unregulated, the targeted allele with the local duplication can revert to either a normal or a mutant allele by postmitotic recombination, and one cannot establish with certainty when the somatic events have occurred. The last point is essential if one seeks to determine whether *polycystin-2* is necessary for the maintenance of tubular morphology or whether its postdevelopmental loss is an important factor in disease progression because the precise time of gene inactiva-

Received March 31, 2004. Accepted August 17, 2004.
Correspondence to Dr. Gregory G. Germino, Johns Hopkins University School of Medicine, Departments of Medicine and Molecular Biology and Genetics, Division of Nephrology, Ross 958, 720 Rutland Avenue, Baltimore, MD 21205. Phone: 410-614-0089; Fax: 410-614-5129; E-mail: ggermino@jhmi.edu
1046-6673/1512-3035
Journal of the American Society of Nephrology

DOI: 10.1097/01.ASN.0000144204.01352.86

tion cannot be defined. In this report, we describe a new line of mice with a floxed allele of *Pkd1* (*Pkd1*$^{cond/cond}$) that functions normally in the undeleted state and results in a null allele after cre-mediated deletion of the intervening sequence.

Materials and Methods

Generation of Pkd1$^{cond/cond}$ *Targeting Construct*

A probe that contained exons 2 to 4 of human *PKD1* was used to screen a lambda bacteriophage library constructed using genomic DNA from the 129sv strain of mice. One clone was found to contain an insert of ~10 kb that included part of intron 1 through exon 15. Detailed genomic mapping and sequencing confirmed that it was collinear with the corresponding segment of mouse genomic DNA. Two adjacent *Eco*RI fragments (3 and 7 kb, respectively) were selected for the backbone of the *Pkd1*^{cond} targeting construct. A neomycin cassette flanked by two *FRT* sites and a single *loxP* site at its 3' end (10) (gift of Dr. Gail R. Martin, University of California at San Francisco, San Francisco, CA) was inserted in a *Bgl*II site of intron 1 (Figure 1A) 1 kb from the 5' end of the targeting vector. Another *loxP* site was placed in an *Xba*I site in intron 4 in the same orientation. The correct orientation and integration of all fragments in the final targeting construct was confirmed by DNA sequence analysis. 129SV-J1 cells were electroporated and subjected to selection of neomycin.

Mouse Lines

The *Pkd1*$^{\beta gal\text{-}null}$ allele has been briefly described elsewhere (11). Briefly, in this line, the bacterial β-galactosidase gene was inserted in place of most of mouse *Pkd1* exon 2 and all of exon 3 by gene targeting. This allele is a true null with transcriptional termination after the β-galactosidase gene but with β-galactosidase expression driven by the native *Pkd1* promoter. Mice homozygous for the *Pkd1*$^{\beta gal\text{-}null}$ allele are embryonic lethal and have hemorrhages and massive edema with polyhydramnios as described previously for other *Pkd1* mutants (5–7). The human β-actin FLPe deleter strain (B6;J-strain TgN[ACTFLPe]9205Dym) expresses a thermostable variant of the yeast *FLP1* recombinase gene under the direction of the human *ACTB* promoter and was a gift of Dr. S.M. Dymecki (Harvard Medical School, Boston, MA) (12). The mouse mamillary tumor virus (MMTV)-Cre (B6129BlSw-TgN[MMTV-Cre]4Mam line) express P1 *Cre* recombinase under the control of the MMTV LTR promoter and was provided by Dr. K.U. Wagner (Eppley Institute for Research in Cancer and Allied Diseases, University of Nebraska Medical Center, Omaha, NE) (13,14). Meox-cre (B6.129S4-*Meox2 tm1[cre]Sor*) transgenic mice were obtained from Jackson Laboratory (15). In this line, the *Cre* recombinase had been "knocked-in" to the *Meox2* gene (mesenchyme homeobox 2 gene) locus. Heterozygotes for *Cre* are phenotypically normal with *Cre* expression regulated by the native promoter of *Meox2*. All studies were performed using approved protocols, and animals were housed and cared for in pathogen-free facilities that are accredited by the American Association for the Accreditation of Laboratory Animal Care and meet federal (National Institutes of Health) guidelines for the humane and appropriate care of laboratory animals.

Genotyping

Genomic DNA was prepared from tail specimens using standard procedures. PCR genotyping was performed using the following primers (Figure 2A): F1, AAT AGG GGT GGG GCT TGT GGG TCG; R3: TGG CGA AAG GGG GAT GTG CTG C; R1, TAC TCA CAC CTC CAC CAG TGC; F2, CTA TAG GAC AGG GAT GAC A; R2, CCC TTA CCA ACC CTC TTT A. *Pkd1* wild-type (and *Pkd1*$^{\beta gal\text{-}null}$) and *Pkd1*^{cond} alleles were identified in 2% 3:1 NuSieve agarose gels as 220- and 250-bp bands, respectively. The *Pkd1*$^{del2\text{–}4}$ allele was detected as a 0.85-kb band *versus* a 1.9-kb nondeleted band in 1% agarose gels (Figure 2A; F3, CGA CCA CCA AGC GAA ACA TC; R4, TCG TGT TCC CTT ACC AAC CCT C). The *Pkd1*$^{cond\text{-}\Delta neo}$ allele was detected by PCR amplification using the primer set shown in Figure 3A (F4, CCT GCC TTG CTC TAC TTT CC; R5, AGG GCT TTT CTT GCT GGT CT). Details regarding PCR conditions are available upon request. Genomic Southern blots of mouse-tail DNA (5 μg/sample) were prepared using standard techniques and probed with P^{32}-labeled probes generated using gel-purified fragments of cloned DNA as template.

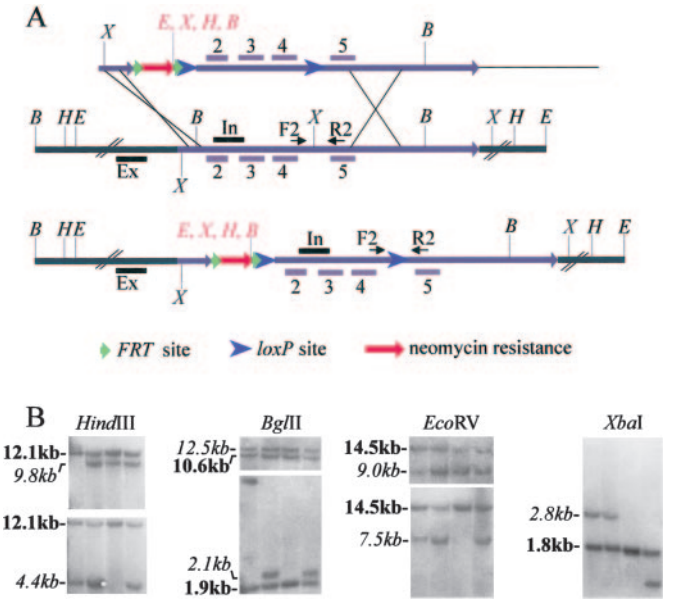

Figure 1. Gene-targeting strategy used to create a floxed allele for murine *Pkd1*. (A) Genomic map and targeting strategy. (Top) Map of the targeting vector. (Middle) Genomic map of wild-type *Pkd1* intron 1-intron 5. (Bottom) The genomic structure of the *Pkd1*^{cond} allele after homologous recombination. The numbers and gray rectangles identify the *Pkd1* exons. "Ex" and "In" identify the 5' external flanking and internal probes used to identify properly targeted alleles by Southern blot. F2 and R2 are primers that amplify a segment of intron 4 into which the lox P site had been introduced in the *Pkd1*^{cond} allele. Single letters identify the following restriction sites: B, *Bgl*II; E, *Eco*RV; H, *Hind*III; X, *Xba*I. (B) Autoradiographs of Southern blots of DNA from four ES clones positive for *Pkd1* gene targeting in the initial screen, digested with the enzymes as shown. The top and bottom panels for each enzyme, except *Xba*I, show the results using the 5' external and internal probes, respectively. The *Xba*I blot was hybridized using only the internal probe. Fragment sizes that correspond to those predicted for the wild-type (bold) and targeted allele (italics) are shown. Clones 2 and 4 (lanes 2 and 4 from the left in each panel) had fragments of the correct size using both probes, but only clone 2 was also correct by *Xba*I mapping. Clone 4 was discarded because it lacked the distal lox P site as indicated by the smaller fragment detected by the internal probe on the *Xba*I blot and confirmed by PCR amplification using primers F2-R2.

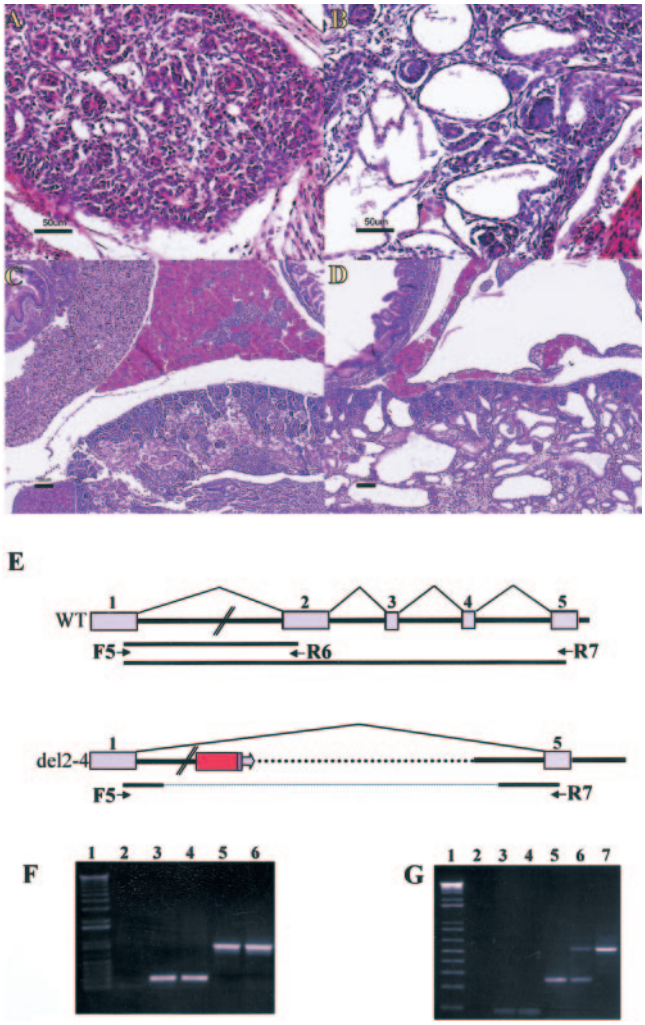

Figure 2. *Pkd1*$^{del2-4}$ homozygotes develop cystic kidneys and pancreas. (A through D) Hematoxylin- and eosin-stained sections of two different E15.5 *Pkd1*$^{del2-4/del2-4}$ embryos (B and D) and wild-type littermates (A and C) showing cystic kidneys (B and D) and pancreas (D) of the mutant animals (A and B, bar = 50 μm; C and D, bar = 100 μm). (E) Schematic drawing showing the genomic map of the wild-type and *Pkd1*$^{del2-4}$ alleles (middle) and their transcripts (top) and the position of primers used to amplify exons 1 to 5 or 1 to 2 (bottom). The colored box indicates the relative position of the neomycin gene (Figure 1A). (F) Genomic PCR of tissues from *Pkd1*$^{del2-4/del2-4}$ (lanes 2 and 5), *Pkd1*$^{del2-4/w}$ (lanes 3 and 6), and *Pkd1*$^{w/w}$ (lane 4) embryos using primers F1-R1 (Figure 4A) to link intron 1 to exon 2. Lane 1 contains the 1-kb Plus marker lane (Invitrogen). *Pkd1*$^{del2-4/del2-4}$ mice lack exon 2 and thus have no product, although other genomic products can be amplified from the same sample with primers F3-R4 (lanes 5 and 6). (G) Reverse transcription–PCR linking exon 1 to more distal exons (exon 2, F5-R6, lanes 2 to 4; exon 5, F5-R7, lanes 5 to 8) in transcripts of *Pkd1*$^{del2-4/del2-4}$ (lanes 2 and 5), *Pkd1*$^{del2-4/w}$ (lanes 3 and 6), and *Pkd1*$^{w/w}$ embryos (lanes 4 and 7). *Pkd1*$^{del2-4/del2-4}$ transcripts lack exons 2 to 4. Lane 1 contains 1-kb Plus marker. The *Pkd1*$^{del2-4/del2-4}$, *Pkd1*$^{del2-4/w}$, and *Pkd1*$^{w/w}$ samples are the same used for lanes 2 to 4 in F. Magnification: ×20 in A and B; ×10 in C and D.

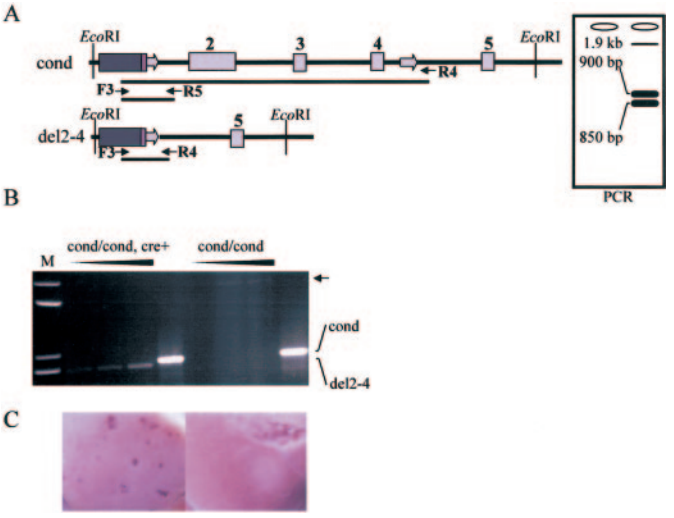

Figure 3. Cre-mediated somatic loss of *Pkd1* results in liver cysts. (A) Schematic illustration of the *Pkd1*^{cond} and *Pkd1*$^{del2-4}$ alleles. The positions of the primer pairs, probe, and restriction enzyme used for Southern blot experiments are as indicated. The predicted sizes for the various products are illustrated in the schematic gel drawing on the right. Primer pair F3-R4 is predicted to yield 1.9- and 0.85-kb fragments from the *Pkd1*^{cond} and *Pkd1*$^{del2-4}$ alleles, respectively, whereas F3-R5 is predicted to yield a 0.9-kb product from both. (B) Ethidium bromide–stained agarose gel with PCR products amplified by the primer pairs shown in A using DNA isolated from paraffin-embedded liver sections of a mouse with the *Pkd1*$^{cond/cond}$:*MMTV-Cre* (cond/cond,cre+) or *Pkd1*$^{cond/cond}$ (cond/cond) genotype as template. The products in the first three lanes for each sample were amplified using increasing amounts of DNA as template and primer pair F3-R4. The prominent product in the last lane of each sample was amplified using primer pair F3-R5 as a positive control to test for DNA quality (cond). A 0.85-kb product (del2–4) was present only in the cystic sample, whereas a 1.9-kb product derived from the undeleted *Pkd1*^{cond} allele was present in the noncystic sample (arrow). (C) Liver specimens used for the PCR reactions in B.

Reverse Transcription–PCR

Total RNA was extracted from fetal tissues using the Qiagen RNA extraction kit according to the manufacturer's protocol. First-strand cDNA was synthesized using Superscript II (Invitrogen) from 100 ng of total RNA and then used as template for PCR amplification of *Pkd1* transcripts (Platinum *Taq*; Invitrogen). Primers F5 (CAG ACG CTA GGG CCG AGT), R6 (CCC TAT GTC CAG CGT CTG AAG TAG), and R7 (TCC AAA GTT CCA GCG TGT TGA) were used to amplify exon 1 to 2 and exon 1 to 5 products, respectively.

Histopathology and Immunohistochemistry

Kidney and liver specimens from adult animals were collected and immediately fixed in 10% buffered formalin at 4°C overnight. Embryos at day 14.5 post coitum were fixed with ice-cold 4% paraformaldehyde in PBS *via* cardiac perfusion of the mother, placed in 4% paraformaldehyde overnight at 4°C, and then transferred to 70% ethanol before embedding in low-melting paraffin. Sections (5 μm) were deparaffinized with xylene and rehydrated in a graded alcohol series. For immunohistochemistry studies, sections were microwaved for 10 min in citrate buffer solution (pH 6.0) to enhance antigen retrieval, preincubated with monoclonal blocker solution (Zymed Lab), and then incubated overnight at 4°C with 1:500 dilution of α-LRR, a monoclonal raised against recombinant human LRR domain. The samples were washed twice with PBST (5 min), and signal

was detected using substrate-chromagen mixture (Zymed Lab). The LRR mAb was purified using the HiTrap protein G HP Mab Trap Kit (Amersham Biosciences).

Ultrasound Imaging

Kidney ultrasound was performed using either a VisualSonics Vevo 660 imaging system with the RVM (real-time microvisualization) 40-MHz scanhead (VisualSonics, Toronto, Ontario, Canada) or a Sequoia C256 (Acuson, Mountain View, CA) imager with 15-MHz linear array transducer. The liver and kidneys were imaged after sedation. After imaging, the animals were killed and their tissues were harvested for gross and histopathologic analysis.

Results

Gene Targeting

A total of 250 clones were picked and screened for gene-targeting events by PCR using a primer anchored in the neomycin gene in combination with one specific for 5' external flanking sequence. Four clones were positive and subjected to extensive mapping by Southern blot analysis using multiple restriction enzymes. Two clones were determined to have undergone internal rearrangements at the *Pkd1* locus, whereas another had lost the single lox P site in intron 4. A single clone was found to have both lox P sites and correct fragment lengths as predicted by the targeting map using 5' and 3' flanking markers as well as several internal probes (Figure 1B). This clone was injected into C57/Bl6 blastocysts, and animals that were obtained from this clone were used in the study. Highly chimeric male mice were mated to black coat color female mice of various backgrounds to confirm germline transmission of the targeted allele with high frequency. Heterozygous $Pkd1^{cond}$ F1 animals were phenotypically normal and exhibited normal reproduction when intercrossed. Typical litter sizes were between six and 10 pups. $Pkd1^{cond}$ homozygotes were obtained at the predicted Mendelian ratio, confirming that the allele was functionally viable (data not shown). Adult $Pkd1^{cond/cond}$ mice were healthy and fertile.

Functional Inactivation of the $Pkd1^{cond}$ Allele

For testing whether the deletion of exons 2 to 4 would result in a functional null allele ($Pkd1^{del2-4}$), heterozygous $Pkd1^{cond}$ F1 mice were bred with *Meox-Cre* transgenic mice to produce $Pkd1^{cond/w}$ male offspring that were also positive for the *Meox-cre* transgene. Expression of the latter results in deletion of floxed DNA segments in >95% of the carrier's germline (15). Thus, the majority of its offspring should have either the $Pkd1^{w}$ or the $Pkd1^{del2-4}$ allele. Given that the homozygous state for null mutations of *Pkd1* results in embryonic lethality, we reasoned that $Pkd1^{del2-4/\beta gal\text{-}null}$ compound heterozygotes also were unlikely to be viable. We tested this hypothesis by setting up a series of 10 crosses between $Pkd1^{cond/w}$:$Meox2^{Cre/w}$ male mice and $Pkd1^{\beta gal\text{-}null/w}$:$Meox2^{w/w}$ female mice and evaluated the genotypes of all liveborn animals. As shown in Table 1, no viable animals were identified with the $Pkd1^{del2-4/\beta gal\text{-}null}$ genotype, and the observed pattern of genotypes differed significantly from what was predicted on the basis of the parental genotypes ($P < 0.001$). We did identify viable animals with the $Pkd1^{del2-4}$ allele, confirming that the cre recombinase was functional and that the targeted allele underwent deletion according to the predicted schema (Figure 4A). We subsequently crossed $Pkd1^{del2-4/w}$ pairs and observed no viable offspring with the $Pkd1^{del2-4/del2-4}$ genotype out of a total of 80 liveborn mice (Table 2).

The lack of viable offspring with the $Pkd1^{del2-4/\beta gal\text{-}null}$ and $Pkd1^{del2-4/del2-4}$ genotypes suggested that either allelic combination resulted in embryonic lethality. To confirm this prediction, we performed a series of timed pregnancies and harvested the litters at 14.5 d post coitum. Figure 4B shows several $Pkd1^{del2-4/\beta gal\text{-}null}$ embryos from a representative litter. Consistent with our hypothesis, $Pkd1^{del2-4/\beta gal\text{-}null}$ embryos exhibited the same phenotype as previously observed for $Pkd1^{\beta gal\text{-}null}$ homozygotes with polyhydramnios, gross total body edema, and hemorrhages commonly observed. Figure 4D shows the genotyping of this particular litter with a schema (Figure 4C) demonstrating the different allele sizes for the PCR as well as the corresponding Southern blot (Figure 4E). It should be noted that no other genotype was associated with an abnormal phenotype *in utero* in these studies. Consistent with these results, day E15.5 $Pkd1^{del2-4/del2-4}$ embryos had similar findings as well as cystic kidneys and pancreas (Figure 2, A through D). Genomic PCR confirmed that mice homozygous for the $Pkd1^{del2-4}$ allele had complete loss of the floxed exons, and reverse transcription–PCR analyses showed that mutant transcripts encoded by the allele lacked exons 2 to 4 (Figure 2, E through G). Tissues of $Pkd1^{del2-4/del2-4}$ embryos also lacked staining for a mAb that recognizes the LRR of human PC-1 (Figure 5). In short, these experiments show conclusively that the $Pkd1^{cond}$ allele leads to a functional null allele when exons 2 to 4 are deleted by cre recombinase.

Somatic Inactivation of Pkd1 Results in Liver and Kidney Cysts

To test whether somatic inactivation of *Pkd1* could result in a detectable phenotype, we cross-bred our heterozygous $Pkd1^{cond}$ F1 animals with *MMTV-cre* transgenic mice. Cre recombinase expression in this transgenic line is under the control of the MMTV promoter and has a mosaic pattern with

Table 1. Genotypes of progeny that result from $Pkd1^{cond/w}$:$Meox2^{cre/w}$ × $Pkd1^{\beta gal\text{-}null/w}$ mating

$PKD1^{w/w}$		$PKD1^{del2-4/w}$		$Pkd1^{\beta gal\text{-}null/w}$		$PKD1^{cond\text{-}del/ko}$	
Observed	Expected	Observed	Expected	Observed	Expected	Observed	Expected
28	19.5	27	19.5	23	19.5	0	19.5

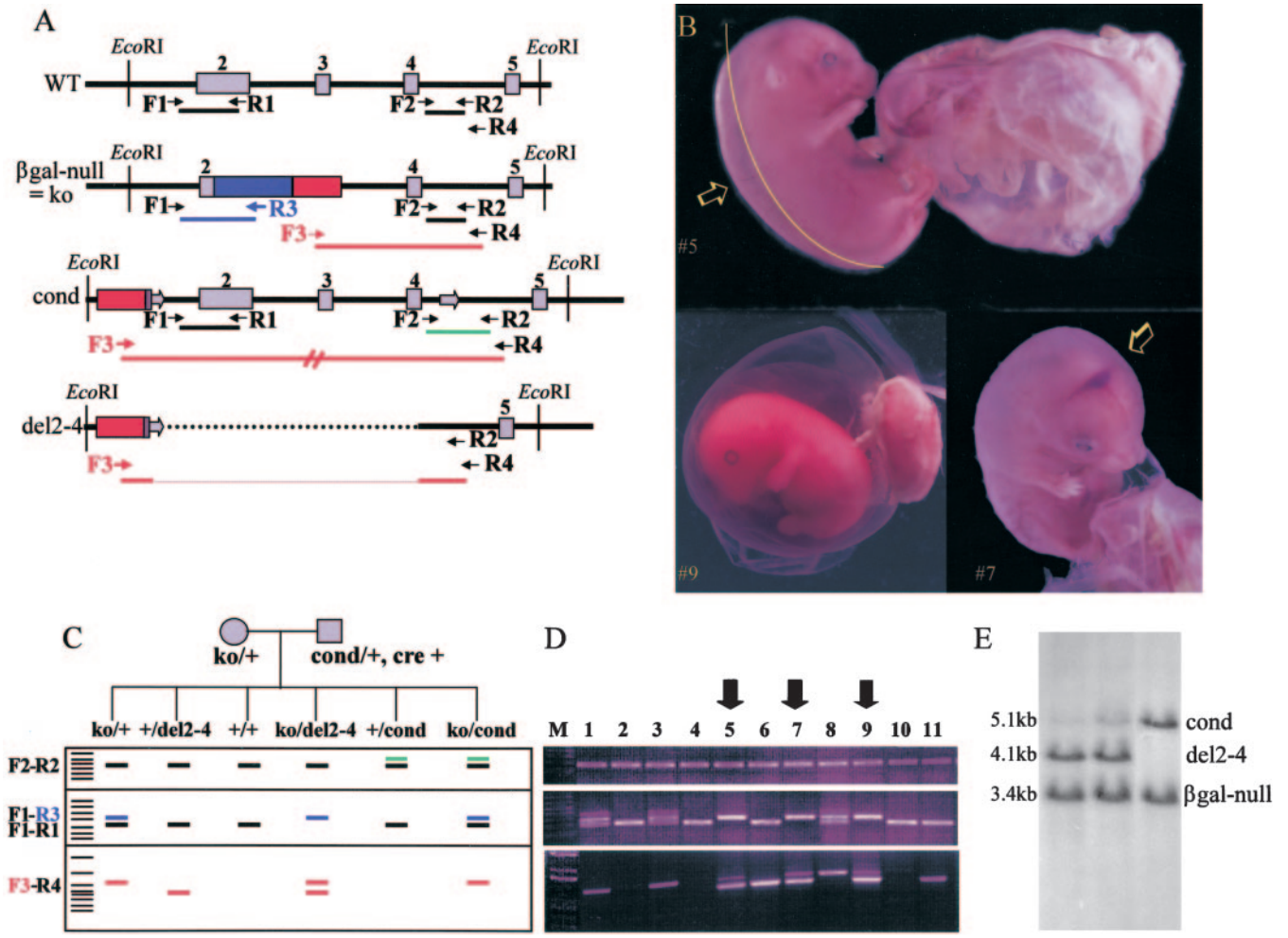

Figure 4. $Pkd1^{del2-4}$ is a functional null allele of *Pkd1*. (A) Schematic drawing of four different alleles that can result from a cross of $Pkd1^{\beta\text{-}gal\text{-}null/w}$:$Meox2^{w/w}$ × $Pkd1^{cond/w}$:$Meox2^{Cre/w}$. WT, wild type; βgal-null, $Pkd1^{\beta gal\text{-}null}$; cond, $Pkd1^{cond}$; del2–4, $Pkd1^{del2-4}$. The positions of the various primer pairs used to confirm the genotypes are as indicated. Black bands are products amplified only from wild-type sequence; blue and red boxes are the β-gal and neomycin genes, respectively. The gray box identifies a slightly longer 3' end for the neomycin gene used in the conditional "ko" construct. The open arrows represent the lox P sites. The long red line with hatches is too long to be amplified under the conditions used. The dashes indicate deleted segments. (B) $Pkd1^{\beta gal\text{-}null/del2-4}$ embryos have the null phenotype. #5 had polyhydramnios and was grossly edematous (arrow in the top picture with a line demonstrating the expected body boundary). #9 had bled into the yolk sac cavity (red haze), and # 7 had a cerebral hemorrhage (arrow). (C) (Top) Schema of breeding strategy and possible allelic combinations that might result. (Bottom) Predicted PCR patterns for each allelic combination. (D) Results obtained for 11 offspring harvested at E14.5. The cre used in this experiment is highly active in the male germline; thus, most offspring have the $Pkd1^{del2-4}$ allele. Three animals (red arrows) were compound heterozygotes for null alleles ($Pkd1^{\beta gal\text{-}null/del2-4}$). No embryos of the $Pkd1^{cond/\beta gal\text{-}null}$ or $Pkd1^{cond/w}$ genotype were present. (F) Autoradiograph of a Southern blot of tail DNA from offspring of a $Pkd1^{\beta gal\text{-}null/w}$:$Meox2^{cre/w}$ × $Pkd1^{cond/w}$:$Meox2^{w/w}$ cross-digested with *Eco*RI and probed with the fragment shown in Figure 7A. The DNA samples in lanes 1 and 2 were isolated from animals with the *Pkd1* null phenotype. A very small amount of undeleted $Pkd1^{cond}$ allele is barely visible in lanes 1 and 2.

Table 2. Genotypes of progeny from mating of $Pkd1^{del2-4/w}$ with $Pkd1^{del2-4/w}$ mice

$PKD1^{w/w}$		$PKD1^{del2-4/w}$		$PKD1^{del2-4/del2-4}$	
Observed	Expected	Observed	Expected	Observed	Expected
30	20	50	40	0	20

low levels of expression in multiple organs, including the kidney (13). This yielded offspring with genotypes of the expected Mendelian ratio. Mice heterozygous for both *MMTV-cre* and $Pkd1^{cond}$ were phenotypically normal in all respects. Brother–sister matings were arranged, and animals of the F2 generation were obtained with genotypes in expected Mende-

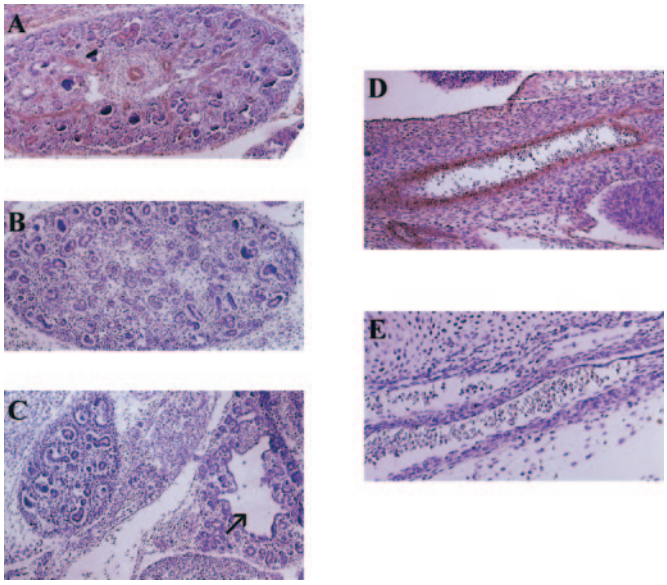

Figure 5. $Pkd1^{del2-4/del2-4}$ embryos lack PC-1. E14.5 $Pkd1^{w/w}$ (A and D) and $Pkd1^{del2-4/del2-4}$ (B, C, and E) stained with α-LRR. (A and D) E14.5 $Pkd1^{w/w}$ kidney and large blood vessel. (B and C) $Pkd1^{del2-4/del2-4}$ kidney and cystic pancreas (arrow). (E) $Pkd1^{del2-4/del2-4}$ large blood vessel. Magnification: ×10 in A, B, and C; ×20 in D and E.

lian ratios. Mice with the $Pkd1^{cond/cond}$:$MMTV^{cre}$ genotype were healthy and reproduced normally.

We selected a set of five animals with the $Pkd1^{cond/cond}$,: $MMTV^{cre}$ genotype and five littermate controls ($Pkd1^{cond/cond}$) for detailed histopathologic analysis at 10 wk of age. Given that ultrasound had previously been used to assess renal cystic disease *in vivo*, we performed a pilot study using a 15-MHz Sequoia linear array transducer on the two sets of animals (16). A single ~3-mm kidney cyst was seen in only one animal ($Pkd1^{cond/cond}$:$MMTV^{cre}$). We then killed the mice and performed post mortem examinations of the kidneys and livers. The cyst that was identified by ultrasound and several smaller cysts were visible on the surface of the organ (Figure 6A). Several small (~1 mm) renal cysts were also visible on the surface of kidneys from two additional mice of the same genotype. The two animals that lacked visible cysts on gross examination also did not have any microscopic cysts detected in a histopathologic survey of 100-μm slices. One of the animals with kidney cysts also had one visible liver cyst of ~4 mm (Figure 6B). None of the control animals, composed of genotypes $Pkd^{cond/w}$:$MMTV^{cre}$, $Pkd1^{w/w}$:$MMTV^{cre}$, or $Pkd1^{cond/cond}$, had any visible or microscopic cysts (Table 3).

To investigate whether a change in phenotype is observed after a longer time period, we analyzed three additional pairs of mice with the $Pkd1^{cond/cond}$ $MMTV^{cre}$ genotype and littermate controls at the age of 20 wk. The kidneys of the first two mice with the $Pkd1^{cond/cond}$ $MMTV^{cre}$ genotype were found on post mortem examination to have bilateral cyst formation with a few cysts in each kidney (Figure 6C). Remarkably, their livers had a marked increase in total cyst number, with >15 cysts in one mouse and >40 in the other (Figure 6D). Most of the cysts

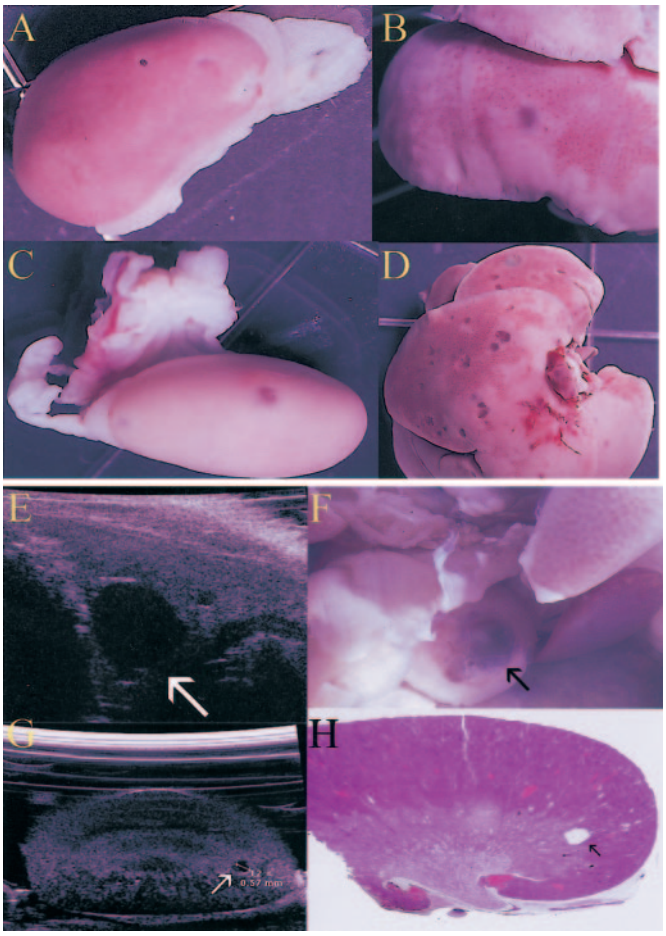

Figure 6. Kidneys and livers of $Pkd1^{cond/cond}$:*MMTV-cre* mice. (A and B) An occasional cyst is visible on the surface of the kidney (A) and liver (B) of 10-wk-old animals. (C and D) Several renal and multiple hepatic cysts are visible on the surface of the organs of 20-wk-old animals. (E and F) High-resolution ultrasound (US) image (40 MHz) and gross appearance of the liver of a 20-wk-old mouse. The arrow identifies the identical cyst present in both images. (G and H) High-resolution US image (40 mHz) and sagittal section of a kidney from a 20-wk-old mouse. The arrow identifies the identical 0.5-mm cyst present in both images not observed on gross examination but detected by sectioning.

were ≥2 mm and of a relatively uniform size. In contrast, none of the kidneys or livers of control animals, composed of genotypes $Pkd1^{cond/w}$:$MMTV^{cre}$, $Pkd1^{w/w}$:$MMTV^{cre}$, or $Pkd1^{cond/cond}$, had any cysts (Table 3).

The last of the pairs was also examined by ultrasound imaging with a recently acquired higher resolution apparatus (40 MHz) before tissue harvesting. Ultrasound detected a cyst of ~0.5 mm on the right kidney and several hepatic cysts, the largest of which was ~3 mm, in the mouse with the $Pkd1^{cond/cond}$ $MMTV^{cre}$ genotype and none in the control (Figure 6, E and G). The initial ultrasound findings were confirmed by the post mortem examination. The liver cysts were immediately visible, and their position and size matched the ultrasound findings. Although the right kidney did not have any visible cysts, the single cyst identified by ultrasound was confirmed by histopathologic analysis of the sectioned tissue (Figure 6, E through H).

Table 3. Overview of liver and kidney phenotypes at 10 and 20 weeks of age in *Pkd1*$^{cond/cond}$*:MMTV-cre/w* and control mice

Genotype	Kidney		Liver	
	10 Weeks (n [cysts$^+$])	20 Weeks (n [cysts$^+$])	10 Weeks (n [cysts$^+$])	20 Weeks (n [cysts$^+$])
PKD1$^{cond/cond}$ MMTV-cre/w	60% (3/5)	100% (3/3)	20% (1/5)	100 (3/3)
All other	0% (0/10)	0% (0/10)	0% (0/10)	0% (0/10)

One possible explanation for the higher rate of cyst formation associated with the *Pkd1*^{cond} allele is that the latter is associated with a higher rate of cyst development by mechanisms other than cre-recombinase–mediated deletion. We tested for this possibility by generating compound heterozygous *Pkd1*$^{cond/\beta gal\text{-}null}$ mice and examining tissues of 6-mo-old animals. None of the organs of eight mice, ranging from 10 to 33 wk of age, had signs of cyst development in either kidney or liver. These results are consistent with what we had previously observed in analyses of >100 heterozygous *Pkd1*$^{\beta gal\text{-}null}$ animals. In this latter set, renal and hepatic cysts were rarely observed in animals 6 mo or younger (unpublished observation).

The clear association between the formation of cysts and the *Pkd1*$^{cond/cond}$*:MMTV*^{cre} genotype suggested that cre-mediated somatic deletion of *Pkd1* was the likely underlying mechanism. To test this hypothesis, we examined cystic and noncystic tissues for the presence of the *Pkd1*$^{del2-4}$ allele. We prepared DNA from sections of cystic liver and from comparable sections of normal liver from control animals and used this as the template for PCR amplification. Two sets of primers were designed for this study (Figure 3A). The first pair flank the floxed segment and produce a 1.9-kb fragment from control specimens and an ~0.85-kb fragment after cre-mediated deletion of exons 2 to 4. Given that we were using paraffin-embedded specimens on glass slides as source material for DNA isolation, we were concerned that the quality of DNA might be suboptimal for reliable amplification of the 1.9-kb fragment. Therefore, we used a second primer (F3-R5; Figure 3A) that was positioned nearby and could amplify a fragment of slightly larger size (0.9 kb) than the deleted fragment from undeleted alleles that could be used as a control for PCR. As shown in Figure 3B, primer pair F3-R4 amplified a 0.85-kb deleted product solely from the cystic specimens, whereas adding primer R5 amplified the 0.9-kb fragment from both cystic and control samples. In contrast, primer pair F3-R4 weakly amplified the 1.9-kb undeleted product from control samples. The lack of 1.9-kb product in the cystic sample likely is the result of preferential amplification of the smaller product.

FRT-Flanked Neomycin Gene of Pkd1^{cond} *Can Be Removed In Vivo*

Most gene-targeting constructs include one or more marker genes that allow selection for the relatively small number of cells that are successfully transfected. In standard "gene knockout" strategies, retention of the selectable marker in the targeted locus after recombination often introduces few problems and may even help ensure successful inactivation of the gene of interest. The risks of untoward effects resulting from a retained marker are far higher when one seeks to develop an allele that can be conditionally inactivated. Even when strategically placed in large introns far from sequences thought essential for proper splicing, the consequences can be unpredictable. Therefore, it is common to flank the selectable marker with additional DNA recombination signals that can be used to delete the marker once it is no longer required. Meyers *et al.* (10) described a novel way of using both *FRT* and *loxP* sites that would allow selective deletion of either the selectable marker or one's targeted gene segment. An advantage of this approach is that it allows for the possible generation of three different alleles (Figure 7A). In situations in which retention of the selectable marker results in a hypomorphic allele, one can potentially use one targeting event to produce a normal, hypomorphic, and completely null allele. Therefore, we had incorporated into the design of our targeting construct FRT sites that flanked the neomycin gene (Figure 1). We had crossed the original *Pkd1*^{cond} chimeric male mice to *FLPe* recombinase female mice to produce *Pkd1*$^{cond/w}$*:FLPe*$^+$ offspring. Southern blot and PCR-based analysis confirmed that the neomycin gene was successfully deleted only in mice that were positive for the *FLPe* transgene, producing a new *Pkd1* allele (*Pkd1*$^{cond\text{-}\Delta neo}$; Figure 7, B and C). However, deletion of the neomycin gene seemed to have no effect on *Pkd1* activity in that the phenotypes of homozygotes for the *Pkd1*^{cond} and *Pkd1*$^{cond\text{-}\Delta neo}$ alleles were identical.

Discussion

In this report, we describe the first line of mice with a floxed allele of a PKD gene (*Pkd1*^{cond}) that functions as a wild-type allele in the undeleted state and as a complete null after cre-mediated deletion. We have shown that mice homozygous for the *Pkd1*^{cond} allele are viable, fertile, and born at the expected Mendelian ratio. In contrast, all previously described lines of animals with targeted mutations of *Pkd1*, including our *Pkd1*$^{\beta gal\text{-}null}$, were either embryonic lethal or had perinatal demise. By breeding *Pkd1*$^{cond/w}$ mice that also were positive for a cre-recombinase to *Pkd1*$^{\beta gal\text{-}null}$ heterozygotes, we could evaluate quickly the functional impact of cre-mediated loss of *Pkd1* exons 2 to 4. As expected, embryos with the *Pkd1*$^{del2-4/\beta\text{-}gal\text{-}null}$ genotype were present in normal Mendelian ratios and recapitulated the range of phenotypes (edema, polyhydramnios, and hemorrhage) associated with homozygous loss of *Pkd1*. These results show conclusively that the

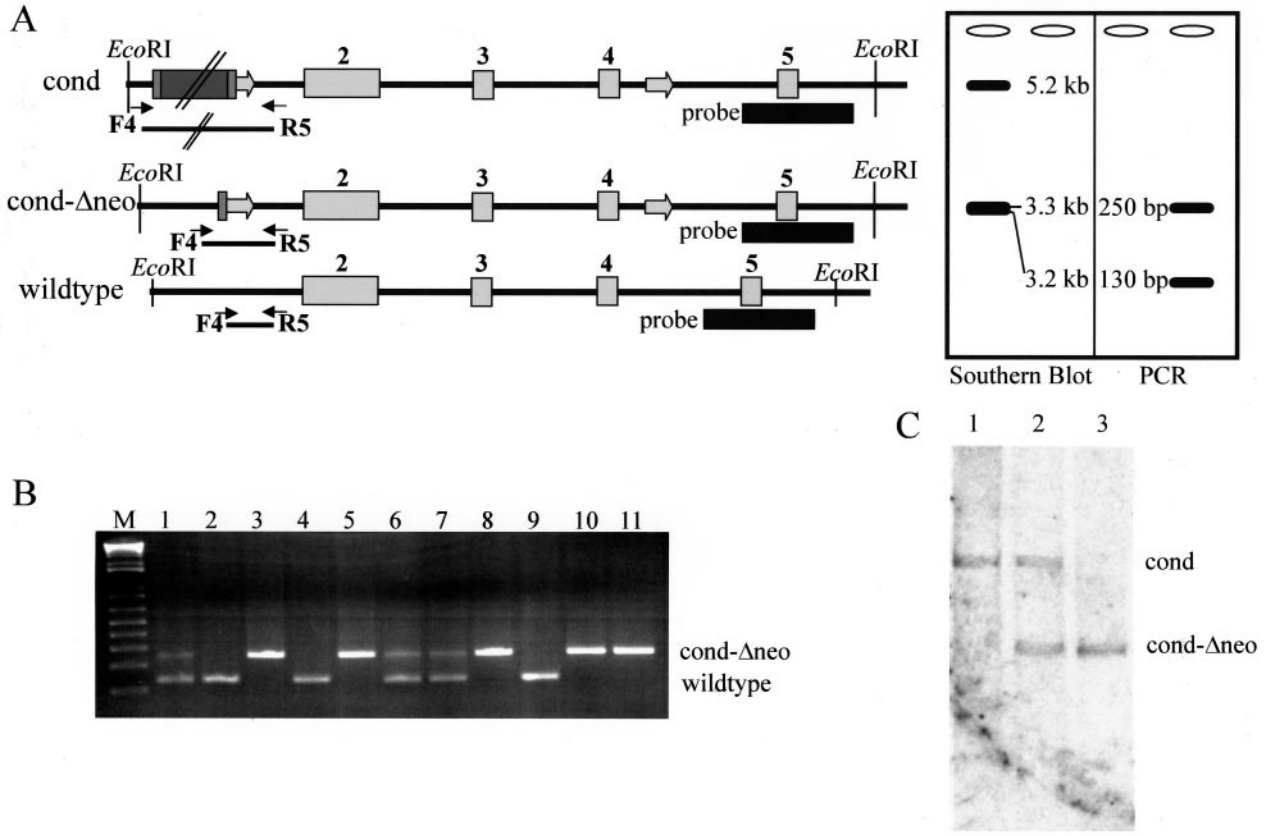

Figure 7. The FLPe-mediated deletion of the neomycin gene from the *Pkd1*^{cond} allele. (A) Schematic illustration of *Pkd1*^{cond} before (cond) and after (cond-Δneo) deletion of the neomycin cassette *via* FLPe-mediated recombination. The primer pair used to distinguish between wild-type and cond-Δneo alleles is indicated, as is the probe and restriction enzyme used for Southern blot experiments. The predicted results for both PCR and Southern blot experiments are illustrated in the schematic gel drawings. The *Pkd1* wild-type allele (3.3 kb) cannot be distinguished from the *Pkd1*$^{cond\text{-}\Delta neo}$ allele (3.2 kb) under the standard conditions used for Southern blotting. (B) Ethidium bromide–stained Nu-Sieve agarose gel with PCR products amplified from tail DNA isolated from offspring of a *Pkd1*$^{cond/w}$:*FLPe*$^{+}$ × *Pkd1*$^{cond/w}$:*FLPe*$^{+}$ mating using F4-R5. The FLPe-recombinase transgene is active in the germline, and the resulting offspring have the *Pkd1*$^{cond\text{-}\Delta neo}$ allele. The samples in lanes 3, 5, 8, 10, and 11 are derived from *Pkd1*$^{cond\text{-}\Delta neo}$ homozygotes. (C) Autoradiograph of a Southern blot of tail DNA digested with *Eco*RI and probed with the fragment shown in A. The genotype of the animals is as follows: lane 1, *Pkd1*$^{cond/cond}$; lane 2, *Pkd1*$^{cond/cond\text{-}\Delta neo}$; lane 3, *Pkd1*$^{cond\text{-}\Delta neo/cond\text{-}\Delta neo}$.

floxed allele functions as a null allele after cre-mediated deletion. Similar results were obtained using mice from different strains, excluding strain differences as a trivial explanation for our findings. In the studies described, all female mice were BlackSwiss/129SVeV F1 hybrids. The male mice were either C57/Bl6/129SVeV (*Pkd1*^{cond}) or BlackSwiss/129SVeV (*Pkd1*$^{\beta gal\text{-}null}$).

An important limitation of the currently available lines of mice with targeted mutations of *Pkd1* is that heterozygous animals rarely have cystic disease below 6 mo of age. For example, $<10\%$ of our *Pkd1*$^{\beta gal\text{-}null}$ heterozygotes ($n > 100$) had macroscopic renal cysts at 3 mo of age, and none had liver cysts at <6 mo of age. It is interesting that mice of this genotype universally develop cystic livers if aged 18 mo or more (unpublished observations). These results are in striking contrast with what is observed in humans, in whom renal cysts are a universal and early finding and liver cysts are acquired later and generally are less abundant. These are important differences that if explained might provide insights into the mechanism of disease. Likewise, it is important that one understand the pathophysiology of disease in the mice models if one seeks to use them to test various therapeutic interventions.

We propose several possible explanations for these species differences. One possibility is that the somatic mutation rate of *PKD1* in human renal and biliary epithelial cells is significantly higher and lower, respectively, than in the corresponding cell types of mice. An alternative explanation is that species differences in the rate of cyst growth in the two organs account for the observations. In this schema, the rate of somatic mutation may not differ, but instead the rates of proliferation or fluid secretion may significantly affect outcome. Finally, it is possible that the molecular mechanisms that govern cyst formation may differ subtly between organisms. The prevailing view regarding the initiation step of cyst formation is that this process begins when some threshold level of PC1/PC2 receptor/channel activity is breached. This can occur as a result of a decrease in the level of activity of the receptor/channel complex and/or an increase in the threshold level required to establish and maintain normal tubule morphology. In heterozy-

gotes, this may result when acquired mutations disrupt the activity of the previously normal allele. It is also possible, however, that the activity of the PC1/PC2 complex normally decreases with age and that in some cell types of heterozygotes it falls below the minimal level. Either the relative level of activity of the complex or the threshold level required to suppress cyst formation in various organs may differ between the species.

The floxed allele of *Pkd1* described in this report can be used to distinguish between these various possibilities. Our studies show that somatic expression of cre recombinase in $Pkd1^{cond/cond}$ mice can result in a null allele and cyst formation. Using this line of animals, one can now examine the consequences of temporally and spatially regulated inactivation of *Pkd1*. By fixing the time and location of gene inactivation, one can examine what other factors affect the relative rate of cyst growth in the kidney and liver. Similarly, by removing the unpredictability of the timing of somatic mutation, this model offers a uniquely powerful way of testing various interventions on the rate of cyst growth. Our pilot study suggests that high-resolution ultrasound imaging may be a useful, noninvasive method for screening for cysts.

This new line of animals also will be invaluable in the study of numerous other aspects of *Pkd1* biology. By controlling the timing of *Pkd1* inactivation, one can show in a definitive way that *Pkd1* is, in fact, necessary for both formation and maintenance of tubules. Likewise, one can use this model to determine the cause of fetal demise. Using this information, one can selectively inactivate the gene in a manner that bypasses the embryonic lethality and then assess the role of PC1 in the development of various other tissues that are altered in *Pkd1* nulls. Finally, one can use this novel model to screen for as-of-yet unidentified postdevelopmental functions of *Pkd1* that are not manifest in humans because of the two-hit nature of disease and not observed in mice because of the early lethality associated with its homozygous loss.

Acknowledgments

This work was funded by the National Institutes of Health (DK48006 to GGG and RR00171 to DLH) and the Johns Hopkins PKD Center of Excellence, sponsored by the National Institute of Diabetes and Digestive and Kidney Diseases. GGG is the Irving Blum Scholar of the Johns Hopkins University School of Medicine.

We thank members of the Germino laboratory for helpful discussions.

References

1. Gabow PA: Autosomal dominant polycystic kidney disease: More than a renal disease. *Am J Kidney Dis* 16: 403–413, 1990
2. Calvet JP: Molecular genetics of polycystic kidney disease. *J Nephrol* 11: 24–34, 1998
3. Qian F, Watnick TJ, Onuchic LF, Germino GG: The molecular basis of focal cyst formation in human autosomal dominant polycystic kidney disease type I. *Cell* 87: 979–987, 1996
4. Wu G, Markowitz GS, Li L, D'Agati VD, Factor SM, Geng L, Tibara S, Tuchman J, Cai Y, Park JH, van Adelsberg J, Hou H Jr, Kucherlapati R, Edelmann W, Somlo S: Cardiac defects and renal failure in mice with targeted mutations in Pkd2. *Nat Genet* 24: 75–78, 2000
5. Lu W, Shen X, Pavlova A, Lakkis M, Ward CJ, Pritchard L, Harris PC, Genest DR, Perez-Atayde AR, Zhou J: Comparison of Pkd1-targeted mutants reveals that loss of polycystin-1 causes cystogenesis and bone defects. *Hum Mol Genet* 10: 2385–2396, 2001
6. Boulter C, Mulroy S, Webb S, Fleming S, Brindle K, Sandford R: Cardiovascular, skeletal, and renal defects in mice with a targeted disruption of the Pkd1 gene. *Proc Natl Acad Sci U S A* 98: 12174–12179, 2001
7. Muto S, Aiba A, Saito Y, Nakao K, Nakamura K, Tomita K, Kitamura T, Kurabayashi M, Nagai R, Higashihara E, Harris PC, Katsuki M, Horie S: Pioglitazone improves the phenotype and molecular defects of a targeted Pkd1 mutant. *Hum Mol Genet* 11: 1731–1742, 2002
8. Pennekamp P, Karcher C, Fischer A, Schweickert A, Skryabin B, Horst J, Blum M, Dworniczak B: The ion channel polycystin-2 is required for left-right axis determination in mice. *Curr Biol* 12: 938–943, 2002
9. Wu G, D'Agati V, Cai Y, Markowitz G, Park JH, Reynolds DM, Maeda Y, Le TC, Hou H Jr, Kucherlapati R, Edelmann W, Somlo S: Somatic inactivation of Pkd2 results in polycystic kidney disease. *Cell* 93: 177–188, 1998
10. Meyers EN, Lewandoski M, Martin GR: An Fgf8 mutant allelic series generated by Cre- and Flp-mediated recombination. *Nat Genet* 18: 136–141, 1998
11. Bhunia AK, Piontek K, Boletta A, Liu L, Qian F, Xu PN, Germino FJ, Germino GG: PKD1 induces p21(waf1) and regulation of the cell cycle via direct activation of the JAK-STAT signaling pathway in a process requiring PKD2. *Cell* 109: 157–168, 2002
12. Rodriguez CI, Buchholz F, Galloway J, Sequerra R, Kasper J, Ayala R, Stewart AF, Dymecki SM: High-efficiency deleter mice show that FLPe is an alternative to Cre-loxP. *Nat Genet* 25: 139–140, 2000
13. Wagner KU, Wall RJ, St-Onge L, Gruss P, Wynshaw-Boris A, Garrett L, Li M, Furth PA, Hennighausen L: Cre-mediated gene deletion in the mammary gland. *Nucleic Acids Res* 25: 4323–4330, 1997
14. Wagner KU, McAllister K, Ward T, Davis B, Wiseman R, Hennighausen L: Spatial and temporal expression of the Cre gene under the control of the MMTV-LTR in different lines of transgenic mice. *Transgenic Res* 10: 545–553, 2001
15. Tallquist MD, Soriano P: Epiblast-restricted Cre expression in MORE mice: A tool to distinguish embryonic vs. extra-embryonic gene function. *Genesis* 26: 113–115, 2000
16. William E, Sweeney JR, Hamahira K, Sweeney J, Garcia-Gatrell M, Frost P, Avner ED: Combination treatment of PKD utilizing dual inhibition of EGF-receptor activity and ligand bioavailability. *Kid Int* 64: 1310–1319, 2003